Ultrasound Tomography Supervised Machine Learning

Gursharan Yash Sandhu[a], Peter Littrup[a,b,c], Mark Sak[a], Cuiping Li[a], Neb Duric[a,b];

[a]Delphinus Medical Technologies, Novi, USA;

[b]Wayne State University, Detroit, USA

[c]Ascension Crittenton Hospital, Rochester, USA

ABSTRACT

Ultrasound tomography generates several different imaging stacks. This includes reflection, sound speed, and attenuation images. The images visualize different acoustic parameters which are useful for assessing different types of breast diseases or tissues. Typically, a radiologist views the images to determine a diagnosis for a patient. However, a learning algorithm can be trained to predict diagnoses based on the features contained within the image. Thus, we present a method to extract features from an ultrasound tomography image and label them. The extracted features with the associated label of benign or malignant are fed to a machine learning algorithm which trains a classifier model (the agent). Extracted features from an unlabeled image are then labeled according to the agent. In particular, the differences in tissue acoustic parameters and lesion heterogeneity within the tumor and its surrounding peritumoral region have great diagnostic potential. Ultimately, a radiologist has to work quickly, thus we will also demonstrate that machine learning tools can be used quickly on clinically relevant time scales.

Keywords: Ultrasound Tomography, Radiomics, Machine Learning, Supervised Learning, Feature Extraction

1. INTRODUCTION

Breast cancer is one of the leading causes of cancer mortality among women.[1,2] Early detection of breast disease can lead to a reduction in the mortality rate.[3] However, problems exist with the sensitivity and specificity of mammography which is the current gold standard for breast cancer screening.[4] These problems are substantial within the subset of young women with dense breasts who are at an increased risk for cancer development.[5] Conventional hand-held ultrasound (HHUS) has proven to be a valuable adjunct to mammography.[6–8] HHUS aids in the detection of cancers in dense breasts and helps differentiate between malignant and benign masses by qualitatively assessing lesion morphology and thus increasing the specificity of diagnostic breast imaging. This leads to reduced anxiety, stress, and physical trauma associated with the biopsy procedure. Problems also exist for HHUS. It is highly operator dependent and difficulties exist for the reproducibility of examinations. It typically only utilizes the basic principles of pulse-echo reflection sonography which cannot use the information contained within the transmitted ultrasound (US) signal. The added cost to the healthcare system as a result of false-positives is also a problem.[9,10]

Ultrasound tomography (UST) might provide a remedy to the deficiencies of HHUS and mammography. Many research groups have investigated the use of reflection and transmission UST.[11–18] In contrast to mammography, UST does not use ionizing radiation or compression. When compared to HHUS, UST is considerably less operator dependent, has more reproducibility of the data acquisition process, and can utilize both reflection and transmission information. UST can utilize reflection signals to create tomographic B-mode images of the breast.[19] The transmitted portion of an US signal contains information about the sound speed and attenuation properties of the insonified medium.[20–25] These properties can aid in the differentiation of fat, fibroglandular tissues, benign masses, and malignant cancer.[20–29] The UST device used for this study and its ring array has been described in our previous work.[30,31]

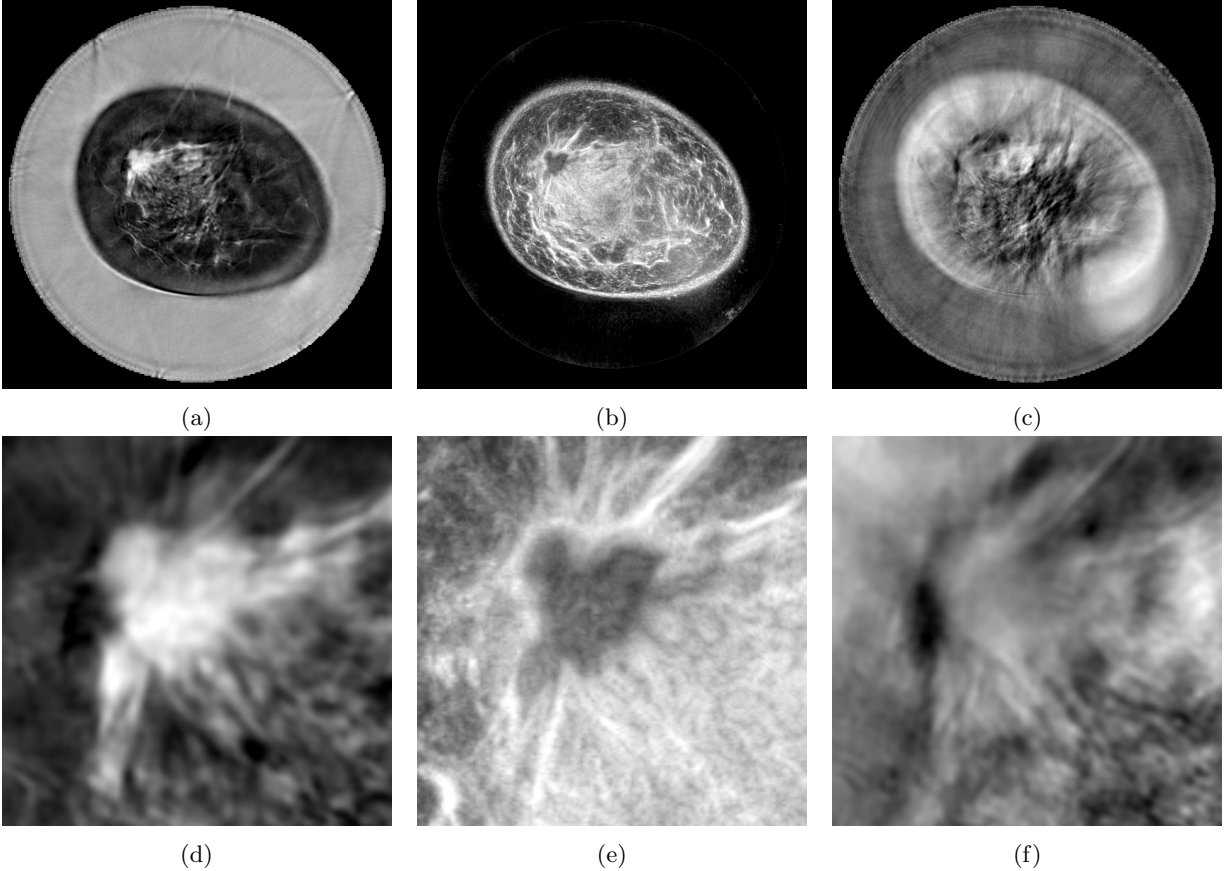Further author information:

gsandhu@delphinusmt.com

Figure 1: Ultrasound tomography images of an invasive ductal carcinoma in the 10:00 position of a breast with scattered parenchymal density. Note tumor location on the interface between fibroglanduar and adipose tissue (IFGA). In contradistinction to benign masses, magnifications views show heterogeneity extending beyond the cancer and into the surrounding peritumoral regions. (a) Sound speed; (b) Reflection; (c) Attenuation; (d) Magnification of Sound Speed; (e) Magnification of Reflection; Magnification of Attenuation.

The goal of developing a UST device is for its eventual application in a clinical setting. There, a radiologist will review the images of a scanned patient and make a diagnosis based on what is seen. In particular, radiologists use their experience and training to make a decision on the presence of any focal imaging abnormality. However, their decision are not always correct, and a possible method to boost their classification ability could utilize radiomic features and classification using supervised machine learning techniques.[32–40] We will focus on assessing breast tissue acoustic parameters and heterogeneity of a breast mass while comparing its tumoral and peritumoral (i.e. surrounding a tumor) regions. For example, in Figure 1, we see an example of the visualization of an invasive ductal carcinoma breast cancer using UST sound speed, reflection, and attenuation images. A magnification of the region surrounding the tumor at 11 o'clock helps define its irregular margins and spiculation. Note the differences in the acoustic parameters and tissue heterogeneity between the tumoral and peritumoral areas. The goal of this paper is to use machine learning techniques to properly classify lesions as benign or malignant based on the differences between these areas. Doing so could improve the classification ability of experienced radiologists as well as boosting novice radiologists so that they perform with increased ability.

In the following sections, we will outline the machine learning method which includes dataset generation for the tumor/peritumoral regions, feature extraction, feature selection, supervised learning, and evaluation metrics. We will show how using different features subsets which correspond to methods which can or can not be done on clinically relevant time scales affect the classification accuracy. We will conclude with our conclusions on the efficacy of the method and future work.
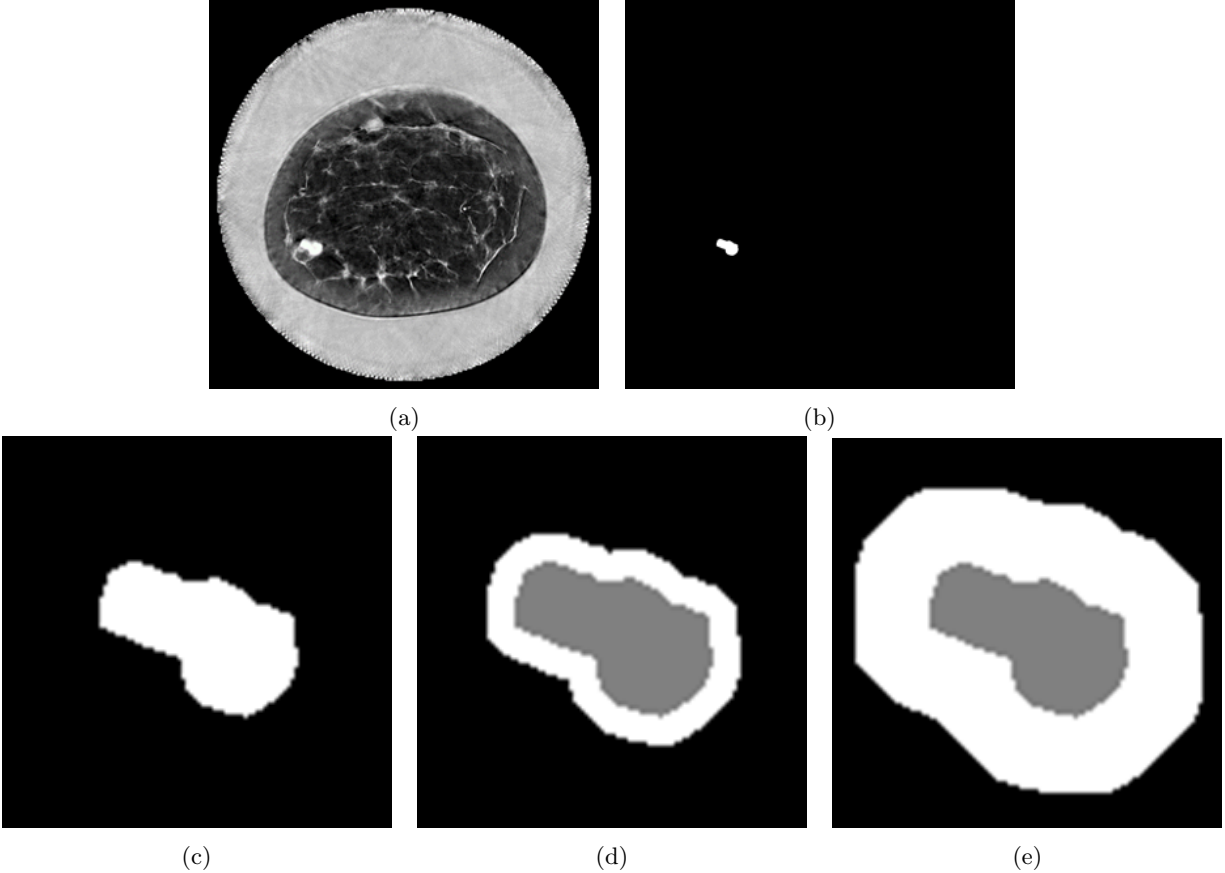
Figure 2: Region-of-Interest (ROI) creation. (a) Sound speed image with a well-circumscribed bilobed fibroadenoma in the peripheral 8:00 position; (b) ROI; (c) Magnification of ROI; (d) ROI with small a peritumoral region. (e) ROI with a larger peritumoral region.

2. METHOD

Tissue characterization of UST images using machine learning techniques requires a series of steps. First, a data set of images must be created which contain examples of different types of tissues and masses. A trained radiologist must then locate and segment the tissue of interest by generating a binary region-of-interest (ROI) mask. Features are then extracted from the ROI. Using feature selection techniques, the most relevant features are then fed to a machine learning classifier model. The trained algorithm can then be fed features from an unknown tissue sample to predict a label for the sample.

2.1 Region of Interest Generation

ROIs are identified within each image which encapsulate a particular tissue or mass. ROI creation is demonstrated in Figure 2. An example of a sound speed image with a well-circumscribed bilobed fibroadenoma in the peripheral 8:00 position is seen in Figure 2a. A mask is drawn around the mass (Figure 2a) to a generate a binary mask as seen in Figures 2b and 2c. The ROI can be expanded to assess features within the surroundings peritumoral region as shown in Figures 2d and 2e. Note, that instead of using a detailed ROI as shown in Figure 2, an elliptical ROI encompassing the lesion could also be created or morphed from the original ROI. For the purposes of this study, we used a data set containing 161 (93 benign and 68 malignant) samples of lesions which includes 38 cysts, 55 fibroadenomas, and 68 cancers.
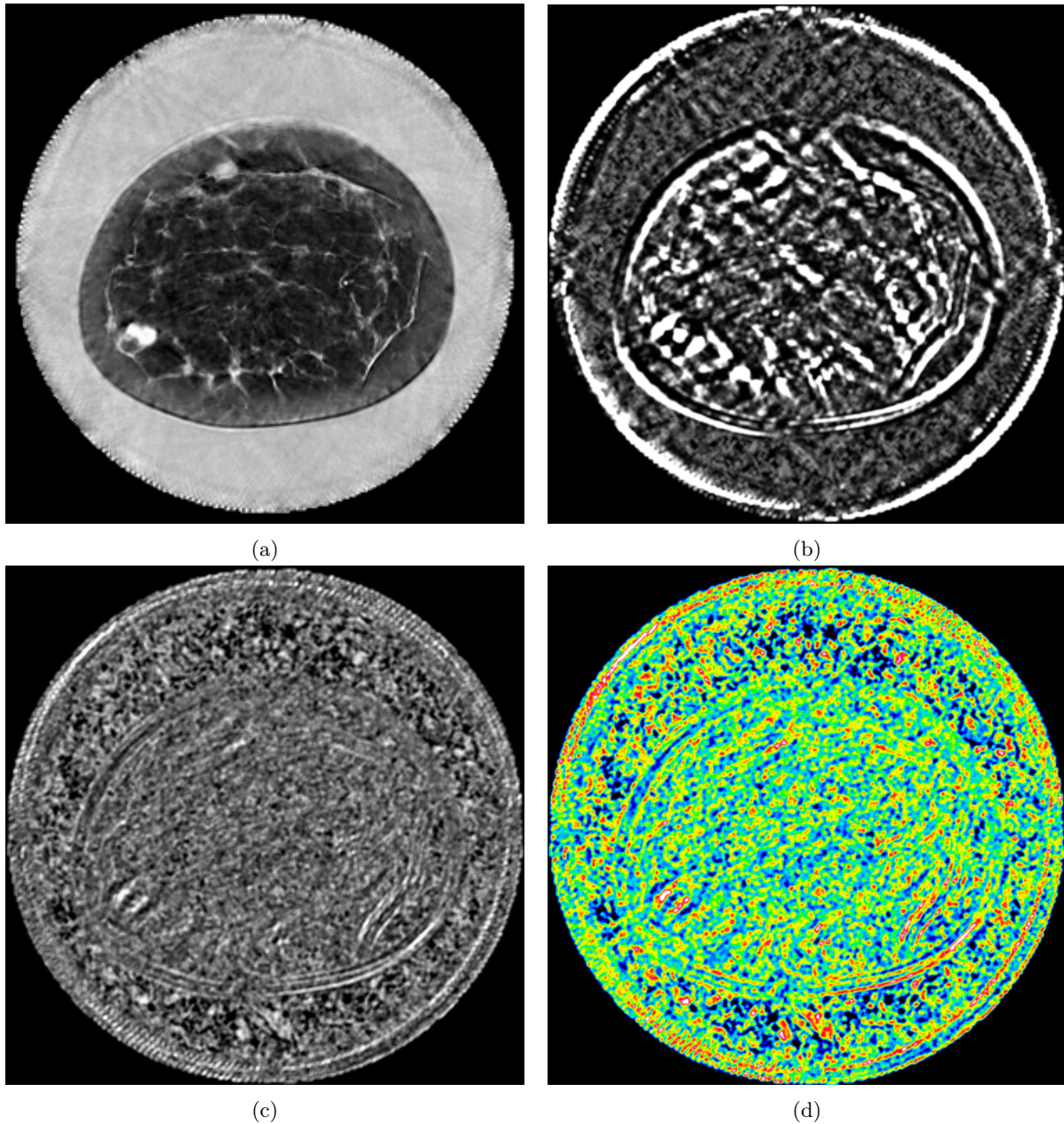
Figure 3: Examples of higher order textural features of the Law's maps. (a) Sound speed image; (b) EE map; (c) ESSE map; (d) ESSE map 4-bit color.

2.2 Feature Extraction

Once an ROI is generated, it can be applied to the various imaging modalities to extract features.[41] Some examples of features include various order statistic assessments of the acoustic parameters or assessments of the texture of the tissue. This includes order statistics such as mean, standard deviation, skewness, etc. Quantitative morphological information can also be obtained from the tumor ROI. Texture metrics include 1st order histogram statistics, 2nd order Gray Level Co-Occurrence Matrix (GLCM) features, as well higher order methods such as texture maps. An example of some of Law's texture maps are seen in Figure 3. Additional features can be extracted from permutations of how the images were contrasted, the differences between the features within the tumor and peritumoral regions, and the imaging type.
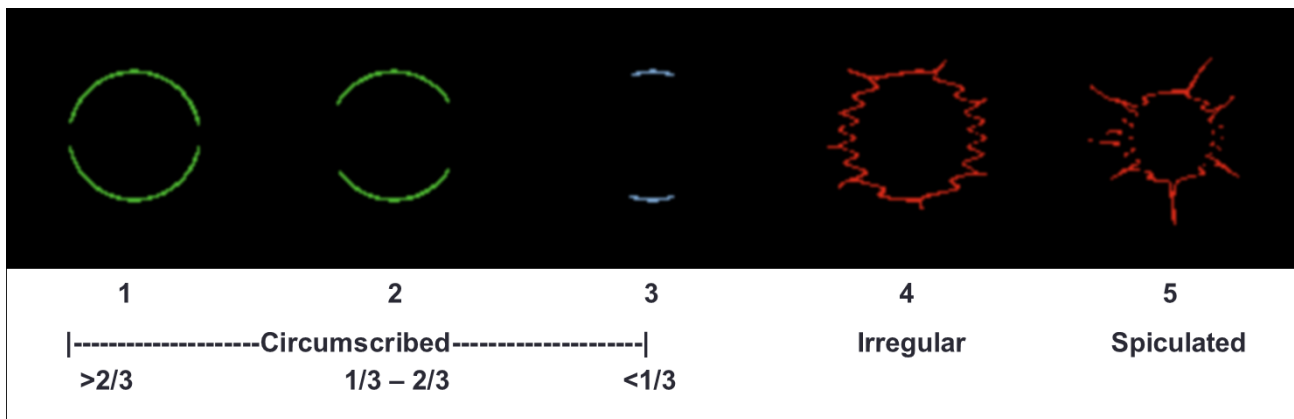
Figure 4: Examples of using the mass boundary score. A lower score reflects more well-defined lesions with circumscribed margins while a higher score reflects more spiculated lesions.

In addition to the features that are extracted from the images, a radiologist could also provide a score that assesses the degree of malignancy. This is crucial as all *a priori* information that can be provided boosts the classification accuracy of a machine learning algorithm.[42] Thus, we have created our own single BI-RADs-like criterion which assesses the degree of heterogeneity in tumor morphology. This score, called the Mass Boundary (MB) score rates a tumor on a scale of 1 to 5. A low value reflects a well circumscribed lesion with well-defined margins while a higher score reflects an irregular or spiculated lesion with ill-defined margins extending into the peritumoral region. An example of this is seen in Figure 4. If greater than 2/3 of the lesion is circumscribed, then a score of 1 is given. If this perimeter is between 1/3 and 2/3, a score of 2 is given. If less than 1/3 of the lesion is circumscribed, then a score of 3 is given. If the lesion is quite irregular, a score of 4 is given. Likewise, if distinct speculations are seen, a score of 5 is given. Therefore, the MB score differs somewhat from an overall BI-RADs score in that the MB score classifies only the tumor/peritumoral morphology and is not meant to convey clinical decision of 12-month follow-up (BI-RADs 1 and 2), 6-month follow-up (BI-RADs 3), or recommendation for biopsy (BI-RADs 4 and 5). Indeed, the MB score likely represents a smoother transition of cancer probability rather than the sharp inflection in probability from <2% with BI-RADs 3 to approximately 10-50% with BI-RADs 4.

2.3 Feature Selection

Given that multiple imaging modalities are used, that we use both the tumor and peritumoral regions, the various contrast choices that can be made, and other permutations, the number of features we obtain quickly explodes to be much greater than the number of patient samples we have. In order to mitigate this dimensionality curse, we must prune the number of features.[43] Some methods to accomplish this include simulated annealing, genetic algorithms, forward selection, backward elimination, and decision tree pruning. We used decision tree pruning to reduce the dimensionality of the hypothesis space. Subsets of features were fed to a decision tree classifier. The top nodes of the trees were aggregated. This allowed reduction in the number of features while keeping features with the greatest information gain.

To demonstrate that machine learning techniques can be used on clinically relevant time scales, we partitioned our features into subcategories. These categories include all acoustic parameter and textural features obtained using a detailed hand-drawn ROI (R), the same features but with a coarse elliptical ROI (RE), quantitative morphological features obtained from the detailed hand-drawn ROI (M), and the mass boundary (MB) score.

2.4 Supervised Learning

Given a vector of features $\vec{x}$ and a label y, the goal of supervised machine learning is to train a classifier model f such that $f(\vec{x}) = y$. In particular, the function f is taught to predict labels by being fed a training set S of features and labels: $S = \{(\vec{x}_1, y_1), (\vec{x}_2, y_2), \ldots, (\vec{x}_N, y_N)\}$. In this manner, the classifier model f does the best job it can on obtaining the proper label. However, the classifier model can be overfitted such that it gives the

proper label for each sample. Thus, a true test of the ability of a classifier model to generalize a data set would lie on its performance on a testing data set.

We tested several classifier models including decision trees, nearest neighbor classifiers, neural networks, support vector machines, and boosted decision stumps.[44–50] Hyperparameter training was done across reasonable parameters until the greatest classification accuracy was obtained. We evaluated both the Weka and scikit-learn machine learning libraries.[51,52]

2.5 Evaluation Metrics

The efficacy of our feature extraction and machine learning method was evaluated by using the sensitivity (SEN), specificity (SPF), and positive predictive value (PPV) of our classifiers. Note that these definitions of SEN, SPF, and PPV are not what they might typically mean for detecting lesions in medical images. Instead, the radiologist has already found the lesion and contoured it. It is the job of the classifier to label the region as benign or malignant. The classifier's SEN, SPF, and PPV thus reflects the ability to properly label the region as benign or malignant. To reduce over-fitting and have a classifier model which generalizes well, it is important to test the classifier on a separate testing set. However, for our testing, the data was not explicitly partitioned into a training and testing set. Instead, a stratified shuffle split cross-validation approach was used. Also, we do not cite the raw SEN, SPF, and PPV values. Instead, we cite the improvement over randomly guessing the classification to better estimate eventual clinical utility.

3. RESULTS

In this section, we will show improvements in SEN, SPF, and PPV over random guessing when using certain subsets of features. The results are seen in Table 1.

Feature Category	SEN	SPF	PPV
R	27.9%	25.1%	34.8%
RE	23.6%	20.8%	29.4%
R + M	31.0%	28.3%	38.9%
R + MB	35.4%	38.0%	51.5%
RE + MB	32.5%	39.1%	52.9%

Table 1: The improvements in sensitivity (SEN), specificity (SPF), and positive predicative value (PPV) over random guessing when using certain categories of features. See Section 2.3 for the definitions of R, RE, M, and MB.

4. CONCLUSIONS

From Table 1, it is seen that using only acoustic parameters and textural information from the UST images generates better classification accuracy over random guessing. This is true when using either the detailed ROI (R) or the elliptical ROI (RE). However, the detailed ROI provides better improvements compared to the elliptical ROI. In addition, if we use a detailed ROI in conjunction with quantitative morphological information obtained from the ROI (R + M), then the classification accuracy improves with respect to not using the morphological information (R). If instead of the quantitative information, we insert additional information from the radiologists in the form of the MB score, the classification accuracy improves further (R + MB). However, since the radiologists assessment of the MB score is such a highly filtering feature, we obtain similar classification accuracy if using an elliptical ROI (RE + MB). Thus, the performance of the detailed ROI and elliptical ROI is comparable (R + MB vs. RE + MB). Since we see vast improvements in classification accuracy over random guessing, we would surmise that machine learning tools will allow a radiologist to boost their ability to assess lesion malignancy. Since the elliptical ROI in conjunction with the MB score performs just as well as the detailed ROI, a radiologist should be able to use machine learning tools on clinically relevant time scales where every click or movement of a mouse is aggregated in terms of clinical cost.

For our future work, we will incorporate a much larger patient data pool. This should improve the classification accuracy which can be seen by developing learning curves from toy datasets such as those available on the

UCI repository.[53] When developing learning curves, one uses increasing fractions of the total data to develop their classifier models. It is typically seen for many problems that the classification accuracy improves as we incorporate more training samples. However, it does eventually saturate. Based on the sample size used in this paper, we should be far away from this saturation point.

5. ACKNOWLEDGMENT

REFERENCES

[1] DeSantis, C., Ma, J., Bryan, L., and Jemal, A., "Breast cancer statistics, 2013," *CA: a cancer journal for clinicians* **64**(1), 52–62 (2014).

[2] Jemal, A., Bray, F., Center, M. M., Ferlay, J., Ward, E., and Forman, D., "Global cancer statistics," *CA: a cancer journal for clinicians* **61**(2), 69–90 (2011).

[3] Leitch, A. M., Dodd, G. D., Costanza, M., Linver, M., Pressman, P., McGinnis, L., and Smith, R. A., "American cancer society guidelines for the early detection of breast cancer: update 1997," *CA: A cancer Journal for Clinicians* **47**(3), 150–153 (1997).

[4] Gøtzsche, P. C. and Olsen, O., "Is screening for breast cancer with mammography justifiable?," *The Lancet* **355**(9198), 129–134 (2000).

[5] Arora, N., King, T. A., Jacks, L. M., Stempel, M. M., Patil, S., Morris, E., and Morrow, M., "Impact of breast density on the presenting features of malignancy," *Annals of surgical oncology* **17**(3), 211–218 (2010).

[6] Berg, W. A., Blume, J. D., Cormack, J. B., Mendelson, E. B., Lehrer, D., Böhm-Vélez, M., Pisano, E. D., Jong, R. A., Evans, W. P., Morton, M. J., et al., "Combined screening with ultrasound and mammography vs mammography alone in women at elevated risk of breast cancer," *Jama* **299**(18), 2151–2163 (2008).

[7] Kolb, T. M., Lichy, J., and Newhouse, J. H., "Comparison of the performance of screening mammography, physical examination, and breast us and evaluation of factors that influence them: an analysis of 27,825 patient evaluations," *Radiology* **225**(1), 165–175 (2002).

[8] Stavros, A. T., Thickman, D., Rapp, C. L., Dennis, M. A., Parker, S. H., and Sisney, G. A., "Solid breast nodules: use of sonography to distinguish between benign and malignant lesions.," *Radiology* **196**(1), 123–134 (1995).

[9] Sprague, B. L., Stout, N. K., Schechter, C., Van Ravesteyn, N. T., Cevik, M., Alagoz, O., Lee, C. I., Van Den Broek, J. J., Miglioretti, D. L., Mandelblatt, J. S., et al., "Benefits, harms, and cost-effectiveness of supplemental ultrasonography screening for women with dense breastssupplemental ultrasonography screening for women with dense breasts," *Annals of internal medicine* **162**(3), 157–166 (2015).

[10] Youk, J. H. and Kim, E.-K., "Supplementary screening sonography in mammographically dense breast: pros and cons," *Korean journal of radiology* **11**(6), 589–593 (2010).

[11] André, M. P., Janée, H. S., Martin, P. J., Otto, G. P., Spivey, B. A., and Palmer, D. A., "High-speed data acquisition in a diffraction tomography system employing large-scale toroidal arrays," *International Journal of Imaging Systems and Technology* **8**(1), 137–147 (1997).

[12] Johnson, S. A., Borup, D. T., Wiskin, J. W., Natterer, F., Wubeling, F., Zhang, Y., and Olsen, S. C., "Apparatus and method for imaging with wavefields using inverse scattering techniques," (Dec. 21 1999). US Patent 6,005,916.

[13] Carson, P. L., Meyer, C. R., Scherzinger, A. L., and Oughton, T. V., "Breast imaging in coronal planes with simultaneous pulse echo and transmission ultrasound," *Science* **214**(4525), 1141–1143 (1981).

[14] Duric, N., Littrup, P., Babkin, A., Chambers, D., Azevedo, S., Kalinin, A., Pevzner, R., Tokarev, M., Holsapple, E., Rama, O., et al., "Development of ultrasound tomography for breast imaging: Technical assessment," *Medical Physics* **32**(5), 1375–1386 (2005).

[15] Liu, D.-L. and Waag, R. C., "Propagation and backpropagation for ultrasonic wavefront design," *IEEE transactions on ultrasonics, ferroelectrics, and frequency control* **44**(1), 1–13 (1997).

[16] Marmarelis, V. Z., Kim, T.-S., and Shehada, R. E., "High resolution ultrasonic transmission tomography," in [*Proc SPIE Med Imaging*], **5035**, 33–40 (2003).

[17] Ruiter, N. V., Göbel, G., Berger, L., Zapf, M., and Gemmeke, H., "Realization of an optimized 3d usct," in [*Proc. SPIE*], **7968**, 796805 (2011).

[18] Greenleaf, J. F., Johnson, S., Bahn, R. C., and Rajagopalan, B., "Quantitative cross-sectional imaging of ultrasound parameters.," in [*Ultrason Symp Proc*], IEEE (1800).

[19] Schmidt, S., Duric, N., Li, C., Roy, O., and Huang, Z.-F., "Modification of kirchhoff migration with variable sound speed and attenuation for acoustic imaging of media and application to tomographic imaging of the breast," *Medical physics* **38**(2), 998–1007 (2011).

[20] Li, C., Duric, N., and Huang, L., "Comparison of ultrasound attenuation tomography methods for breast imaging," *Ultrasonic Imaging and Signal Processing], McAleavey, SA and Dhooge, J., eds., Proc. SPIE* **6920**, 692015–1 (2008).

[21] Li, C., Duric, N., and Huang, L., "Clinical breast imaging using sound-speed reconstructions of ultrasound tomography data," *Ultrasonic Imaging and Signal Processing], McAleavey, SA and Dhooge, J., eds., Proc. SPIE* **6920**, 692009–1 (2008).

[22] Li, C., Duric, N., Littrup, P., and Huang, L., "In vivo breast sound-speed imaging with ultrasound tomography," *Ultrasound in medicine & biology* **35**(10), 1615–1628 (2009).

[23] Sandhu, G., Li, C., Roy, O., Schmidt, S., and Duric, N., "Frequency domain ultrasound waveform tomography: breast imaging using a ring transducer," *Physics in medicine and biology* **60**(14), 5381 (2015).

[24] Sandhu, G. Y., Li, C., Roy, O., Schmidt, S., and Duric, N., "High-resolution quantitative whole-breast ultrasound: in vivo application using frequency-domain waveform tomography," in [*Proc. SPIE*], **9419**, 94190D (2015).

[25] Sandhu, G. Y. S., Li, C., Roy, O., West, E., Montgomery, K., Boone, M., and Duric, N., "Frequency-domain ultrasound waveform tomography breast attenuation imaging," in [*Medical Imaging 2016: Ultrasonic Imaging and Tomography*], **9790**, 97900C, International Society for Optics and Photonics (2016).

[26] Duck, F. A., [*Physical properties of tissues: a comprehensive reference book*], Academic press (2013).

[27] Edmonds, P., Mortensen, C., Hill, J., Holland, S., Jensen, J., Schattner, P., Valdes, A., Lee, R., and Marzoni, F., "Ultrasound tissue characterization of breast biopsy specimens," *Ultrasonic imaging* **13**(2), 162–185 (1991).

[28] Goss, S., Johnston, R., and Dunn, F., "Comprehensive compilation of empirical ultrasonic properties of mammalian tissues," *The Journal of the Acoustical Society of America* **64**(2), 423–457 (1978).

[29] Boyd, N. F., Martin, L. J., Bronskill, M., Yaffe, M. J., Duric, N., and Minkin, S., "Breast tissue composition and susceptibility to breast cancer," *Journal of the National Cancer Institute* **102**(16), 1224–1237 (2010).

[30] Duric, N., Littrup, P., Schmidt, S., Li, C., Roy, O., Bey-Knight, L., Janer, R., Kunz, D., Chen, X., Goll, J., et al., "Breast imaging with the softvue imaging system: First results," in [*Proc. SPIE*], **8675**, 86750K (2013).

[31] Roy, O., Schmidt, S., Li, C., Allada, V., West, E., Kunz, D., and Duric, N., "Breast imaging using ultrasound tomography: From clinical requirements to system design," in [*Ultrasonics Symposium (IUS), 2013 IEEE International*], 1174–1177, IEEE (2013).

[32] Ranger, B., Littrup, P. J., Duric, N., Chandiwala-Mody, P., Li, C., Schmidt, S., and Lupinacci, J., "Breast ultrasound tomography versus mri for clinical display of anatomy and tumor rendering: preliminary results," *American Journal of Roentgenology* **198**(1), 233–239 (2012).

[33] Honda, E., Nakayama, R., Koyama, H., and Yamashita, A., "Computer-aided diagnosis scheme for distinguishing between benign and malignant masses in breast dce-mri," *Journal of digital imaging* **29**(3), 388–393 (2016).

[34] Davnall, F., Yip, C. S., Ljungqvist, G., Selmi, M., Ng, F., Sanghera, B., Ganeshan, B., Miles, K. A., Cook, G. J., and Goh, V., "Assessment of tumor heterogeneity: an emerging imaging tool for clinical practice?," *Insights into imaging* **3**(6), 573–589 (2012).

[35] Sutton, E. J., Oh, J. H., Dashevsky, B. Z., Veeraraghavan, H., Apte, A. P., Thakur, S. B., Deasy, J. O., and Morris, E. A., "Breast cancer subtype intertumor heterogeneity: Mri-based features predict results of a genomic assay," *Journal of Magnetic Resonance Imaging* **42**(5), 1398–1406 (2015).

[36] Malik, B., Klock, J., Wiskin, J., and Lenox, M., "Objective breast tissue image classification using quantitative transmission ultrasound tomography," *Scientific reports* **6**, 38857 (2016).

[37] Li, H., Zhu, Y., Burnside, E. S., Huang, E., Drukker, K., Hoadley, K. A., Fan, C., Conzen, S. D., Zuley, M., Net, J. M., et al., "Quantitative mri radiomics in the prediction of molecular classifications of breast cancer subtypes in the tcga/tcia data set," *NPJ breast cancer* **2** (2016).

[38] Li, H., Zhu, Y., Burnside, E. S., Drukker, K., Hoadley, K. A., Fan, C., Conzen, S. D., Whitman, G. J., Sutton, E. J., Net, J. M., et al., "Mr imaging radiomics signatures for predicting the risk of breast cancer recurrence as given by research versions of mammaprint, oncotype dx, and pam50 gene assays," *Radiology* **281**(2), 382–391 (2016).

[39] Gillies, R. J., Kinahan, P. E., and Hricak, H., "Radiomics: images are more than pictures, they are data," *Radiology* **278**(2), 563–577 (2015).

[40] Street, W. N., Wolberg, W. H., and Mangasarian, O. L., "Nuclear feature extraction for breast tumor diagnosis," in [*IS&T/SPIE's Symposium on Electronic Imaging: Science and Technology*], 861–870, International Society for Optics and Photonics (1993).

[41] Jain, R., Kasturi, R., and Schunck, B. G., [*Machine vision*], vol. 5, McGraw-Hill New York (1995).

[42] Ho, Y.-C. and Pepyne, D. L., "Simple explanation of the no-free-lunch theorem and its implications," *Journal of optimization theory and applications* **115**(3), 549–570 (2002).

[43] Blum, A. L. and Langley, P., "Selection of relevant features and examples in machine learning," *Artificial intelligence* **97**(1), 245–271 (1997).

[44] Quinlan, J. R., [*C4. 5: programs for machine learning*], Elsevier (2014).

[45] Breiman, L., Friedman, J. H., Olshen, R. A., and Stone, C. J., "Classification and regression trees. wadsworth & brooks," *Monterey, CA* (1984).

[46] Indyk, P. and Motwani, R., "Approximate nearest neighbors: towards removing the curse of dimensionality," in [*Proceedings of the thirtieth annual ACM symposium on Theory of computing*], 604–613, ACM (1998).

[47] Hecht-Nielsen, R. et al., "Theory of the backpropagation neural network.," *Neural Networks* **1**(Supplement-1), 445–448 (1988).

[48] Burges, C. J., "A tutorial on support vector machines for pattern recognition," *Data mining and knowledge discovery* **2**(2), 121–167 (1998).

[49] Schapire, R. E., "The boosting approach to machine learning: An overview," in [*Nonlinear estimation and classification*], 149–171, Springer (2003).

[50] Mitchell, T. M. et al., "Machine learning. WCB," (1997).

[51] Hall, M., Frank, E., Holmes, G., Pfahringer, B., Reutemann, P., and Witten, I. H., "The weka data mining software: an update," *ACM SIGKDD explorations newsletter* **11**(1), 10–18 (2009).

[52] Pedregosa, F., Varoquaux, G., Gramfort, A., Michel, V., Thirion, B., Grisel, O., Blondel, M., Prettenhofer, P., Weiss, R., Dubourg, V., Vanderplas, J., Passos, A., Cournapeau, D., Brucher, M., Perrot, M., and Duchesnay, E., "Scikit-learn: Machine learning in Python," *Journal of Machine Learning Research* **12**, 2825–2830 (2011).

[53] Lichman, M., "UCI machine learning repository," (2013).